From κ to χ: Evaluating Hygroscopicity-Based Mixing State Estimates with a Particle-Resolved Model

Yicen Liu[a], Jian Wang[b], and Nicole Riemer[c]

[a]Department of Civil and Environmental Engineering, Grainger College of Engineering, University of Illinois Urbana-Champaign, Urbana, IL, USA
[b]Department of Energy, Environmental, and Chemical Engineering, Washington University in St. Louis, St. Louis, MO, USA
[c]Department of Climate, Meteorology, and Atmospheric Science, University of Illinois Urbana-Champaign, Urbana, IL, USA

Correspondence: Nicole Riemer (nriemer@illinois.edu)

Abstract. Aerosol mixing state strongly influences how particles interact with clouds, radiation, and atmospheric chemistry, but it remains difficult to quantify from routine observations. The aerosol mixing state index (χ) typically requires detailed single-particle composition data, available only from particle-resolved models or advanced measurements. Yuan and Zhao (2023) proposed estimating χ from in-situ hygroscopicity (κ) measurements using a hygroscopicity tandem differential mobility analyzer (HTDMA), offering a promising observational pathway. However, their method assumes a binary system of more- and less-hygroscopic components, which may not represent aerosol populations containing intermediate-hygroscopicity species. Here, we systematically evaluate this κ-based χ retrieval using the stochastic particle-resolved model PartMC-MOSAIC. We generated a large ensemble of aerosol populations from urban plume simulations spanning a wide range of emissions, aging conditions, and meteorology. For each population and particle diameter (50–250 nm), we compared the particle-resolved reference mixing state index from per-particle composition (χ^{PMC}) with the χ inferred from κ distributions using the Yuan–Zhao method (χ^{YZ}). The retrieval performs well for many aerosol populations, but systematically overestimates χ when externally mixed intermediate-hygroscopicity components violate the binary assumption. By quantifying the error distributions across particle sizes, we derive uncertainty bounds for the retrieval and apply them to long-term HTDMA datasets from urban, continental, and coastal sites, providing a first multi-site assessment of seasonal variability in χ inferred from hygroscopicity measurements.

1 Introduction

Atmospheric aerosols are complex mixtures of different chemical species. The chemical composition of aerosols governs their role in key atmospheric processes, including the ability to act as cloud condensation nuclei (CCN) (Hallberg et al., 1994; Leck et al., 2002; Cubison et al., 2008; Leck and Svensson, 2015), interactions with incoming solar radiation (Patterson, 1981; Ravishankara et al., 2015; Drame et al., 2015), and capacity to facilitate heterogeneous reactions (George and Abbatt, 2010; H. Bertram et al., 2018; Baustian et al., 2012). These processes depend not only on the bulk chemical composition but also on how different chemical species are distributed among and within individual particles, a characteristic termed the aerosol mixing state (Riemer and West, 2013). Aerosol populations can be "internally mixed", where all particles possess the same

composition as the bulk, or "externally mixed", where each particle consists of a single chemical species. However, field measurements reveal that real atmospheric aerosols fall between these two extremes, exhibiting complex mixing states that evolve through processes such as coagulation, condensation, chemical aging, and transport (Laskin et al., 2002; Ebert et al., 2004; Kleinman et al., 2008; Li et al., 2010; Sun et al., 2013; Adachi et al., 2022; Yoo et al., 2024).

To quantify the degree of internal versus external mixing, Riemer and West (2013) proposed the aerosol mixing state index (χ), which applies information-theoretic (Shannon) entropy to the distribution of chemical species among particles based on per-particle mass fractions. For any aerosol population, χ ranges from 0% (fully external mixture) to 100% (fully internal mixture). The metric has been applied to evaluate the mixing state assumptions for air quality modeling (Zhu et al., 2016), examine the evolution of particle mixing structure (Li et al., 2016), and assess mixing state heterogeneity impacts on black carbon light absorption enhancement (Zeng et al., 2024). Direct calculation of χ requires detailed single-particle composition data, which can be obtained through either single-particle measurement techniques or particle-resolved models.

While several studies have successfully computed χ using single-particle techniques such as aerosol time-of-flight mass spectrometry (ATOFMS), computer-controlled scanning electron microscopy/energy dispersive X-ray spectroscopy (CCSEM/EDX), Scanning Transmission X-ray Microscopy/Near Edge Fine Structure spectroscopy (STXM/NEXAFS) (Wu et al., 2024; O'Brien et al., 2015; Fraund et al., 2017; Bondy et al., 2018; Lata et al., 2021; Singh et al., 2021; M. Tomlin et al., 2022; Cheng et al., 2023; Xue et al., 2024a; Sharpe et al., 2025; Rivera-Adorno et al., 2025), and single-particle soot photometer (SP2) (Yu et al., 2020; Zhao et al., 2021a), they remain relatively rare and campaign-specific. Similarly, particle-resolved models such as PartMC-MOSAIC (Particle Monte Carlo-Model for Simulating Aerosol Interactions and Chemistry) have been used to compute χ and investigate mixing state evolution (Shou et al., 2019; Gasparik et al., 2020; Zheng et al., 2021; Yao et al., 2022; Jiang et al., 2025; Zhang et al., 2025), but are computationally intensive and cannot be applied directly to observational datasets without extensive additional information. These limitations motivate a shift toward approaches that infer χ from more routinely available aerosol measurements.

Hygroscopicity measurements offer a promising way to infer aerosol mixing state. Aerosol hygroscopicity describes the ability of particles to take up water, and its dependence on chemical composition is characterized by the hygroscopicity parameter (κ) (Petters and Kreidenweis, 2007). The κ value can be obtained from the hygroscopic growth factors using a hygroscopic Tandem Differential Mobility Analyzer (HTDMA) (Rader and McMurry, 1986) under subsaturated conditions, and are widely deployed at monitoring networks and field campaigns (Mochida et al., 2010; Adam et al., 2012; Yeung et al., 2014; Zhang et al., 2017; Phillips et al., 2018; Wang and Chen, 2019; Tao et al., 2023; Deshmukh et al., 2025). Importantly, HTDMA measurements yield not only mean κ values but also probability distributions of κ (κ-PDFs), which capture particle-to-particle heterogeneity in aerosol hygroscopicity while bypassing the need for single-particle composition data.

Accordingly, Yuan and Zhao (2023) proposed an elegant method (hereafter referred to as YZ) to infer χ from HTDMA-measured κ-PDFs. In brief, YZ assumes that aerosols are binary mixtures of more-hygroscopic (MH) and less-hygroscopic (LH) components with distinct κ values, such that the measured κ-PDF can be mapped to the distribution of MH/LH volume fractions, from which χ is computed. A key limitation is that the binary assumption may be violated in real atmospheric populations, as many aerosols may contain intermediate-hygroscopicity components, (e.g., secondary organic aerosol, SOA)

that do not fit neatly into either MH or LH categories. This oversimplification of chemical variability may introduce systematic biases in χ estimates.

While the YZ method offers a practical approach, its performance under realistic atmospheric conditions remains poorly understood, particularly when particles contain substantial fractions of intermediate-hygroscopicity material. It is therefore unclear how large the bias in inferred χ might be, under what conditions the method remains reliable, and when it begins to break down. These knowledge gaps raise questions about whether χ derived from κ-PDFs can be applied confidently to long-term field datasets.

In this work, we evaluate the YZ method with particle-resolved simulations across diverse atmospheric conditions and particle sizes, quantifying both its accuracy and systematic biases associated with the assumption made to derive χ. By benchmarking the YZ method against particle-resolved simulations, we identify the regimes in which κ-derived χ can be interpreted with confidence, as well as conditions under which the underlying binary hygroscopicity assumption introduces systematic bias. We then apply the YZ method to long-term HTDMA measurements from four campaigns within the U.S. Department of Energy's Atmospheric Radiation Measurement (ARM) program. This study establishes the systematic evaluation of χ derived from κ-only measurements and quantifies uncertainty ranges for κ-based mixing state retrievals, providing foundations for climatological applications.

The paper is structured as follows: Section 2 revisits the YZ algorithm, and Section 3 describes the particle-resolved model, validation scenario library, and HTDMA datasets. Section 4 examines the relationship between particle-resolved reference χ from per-particle composition and estimated χ using the YZ κ-based method. Section 5 presents κ-based χ retrievals in field measurements.

2 Hygroscopicity-Based Aerosol Mixing State Metric (χ)

The YZ method assumes each aerosol particle in the population consists of one or both of MH and LH components, with κ calculated as the volume-weighted average of κ_{LH} and κ_{MH}. For the aerosol with a given dry diameter and a known κ-PDF with X κ-bins, the volume fractions of the LH ($P_{i,\mathrm{LH}}$) and MH ($P_{i,\mathrm{MH}}$) components at bin i ($i =$ 1, 2, 3, ..., X) can be calculated as:

$$P_{i,\mathrm{MH}} = \frac{\kappa_i - \kappa_{\mathrm{LH}}}{\kappa_{\mathrm{MH}} - \kappa_{\mathrm{LH}}}, \tag{1}$$

$$P_{i,\mathrm{LH}} = 1 - P_{i,\mathrm{MH}}, \tag{2}$$

where κ_i is the κ at bin i.

The original YZ method used $\kappa_{\mathrm{LH}} = 0.01$ and $\kappa_{\mathrm{MH}} = 0.6$. In our simulations, we expanded these bounds to $\kappa_{\mathrm{LH}} = 0$ (for nearly hydrophobic components such as BC) and $\kappa_{\mathrm{MH}} = 0.65$ (for highly hygroscopic inorganic species such as $\mathrm{SO_4}$, $\mathrm{NO_3}$, and $\mathrm{NH_4}$). Expanding the bounds ensures that we capture the full spectrum of particle hygroscopicity simulated in PartMC. For

future applications, these bounds can be flexibly chosen based on measured κ distributions from HTDMA, so that the binary system captures the observed range of hygroscopicities in the ambient aerosol population.

Particles selected by the HTDMA at a given dry diameter exhibit a finite size distribution determined by the DMA transfer function (Brechtel and Kreidenweis, 2000; Collins et al., 2004). The YZ method neglects this residual size dispersion and assumes that particles assigned to the same κ-bin are effectively monodisperse within instrumental resolution. Under this approximation, they are treated as having identical physicochemical properties and mixing entropy. The entropies can be obtained from the normalized κ-PDF:

$$H_i = -P_{i,\mathrm{LH}} \times \ln P_{i,\mathrm{LH}} - P_{i,\mathrm{MH}} \times \ln P_{i,\mathrm{MH}}, \tag{3}$$

$$H_\alpha = \sum_{i=1}^{X} H_i \times c(\kappa)_i \times \Delta\kappa, \tag{4}$$

$$H_\gamma = -P_{\mathrm{LH}} \times \ln P_{\mathrm{LH}} - P_{\mathrm{MH}} \times \ln P_{\mathrm{MH}}, \tag{5}$$

where $c(\kappa)_i$ is the probability density value of the normalized κ-PDF at bin i, and $\Delta\kappa$ is the bin width, P_{LH} and P_{MH} are the respective volume fraction of the LH and MH components in the population, and they can be calculated by:

$$P_{\mathrm{LH}} = \sum_{i=1}^{X} P_{i,\mathrm{LH}} \times c(\kappa)_i \times \Delta\kappa \tag{6}$$

and

$$P_{\mathrm{MH}} = \sum_{i=1}^{X} P_{i,\mathrm{MH}} \times c(\kappa)_i \times \Delta\kappa \tag{7}$$

The species diversities are calculated from the mixing entropies as:

$$D_i = e^{H_i}, \tag{8}$$

$$D_\alpha = e^{H_\alpha}, \tag{9}$$

and

$$D_\gamma = e^{H_\gamma}, \tag{10}$$

with D_i, D_α, and D_γ denote the diversity of the particle subpopulation represented by the i^{th} κ-bin, average per-bin diversity, and bulk population diversity, respectively.

The hygroscopicity-based aerosol mixing state index χ can be calculated as:

$$\chi = \frac{D_\alpha - 1}{D_\gamma - 1}, \tag{11}$$

which varies from 0% that all particles in the population purely consist of the LH or MH component to 100% that the LH and MH components are homogeneously distributed across all particles in the population with identical volume fractions.

3 Ensemble of Particle-Resolved Model Scenarios

3.1 PartMC-MOSAIC Model Description

PartMC (Particle-resolved Monte Carlo) (Riemer et al., 2009) is a stochastic, zero-dimensional aerosol model that simulates the evolution of per-particle composition of an aerosol population within a well-mixed computational volume. The particle positions within the computational volume are not tracked. The composition of individual particles evolves through emission, dilution, and coagulation, modeled using a stochastic Monte Carlo approach. Dry and wet deposition of aerosol particles are not included.

To allow for the treatment of aerosol chemistry, PartMC is coupled to the aerosol chemistry model MOSAIC (Model for Simulating Aerosol Interactions and Chemistry) (Zaveri et al., 2008). This includes the gas phase photochemical mechanism CBM-Z (Carbon-Bond Mechanism) (Zaveri and Peters, 1999), the Multicomponent Taylor Expansion Method (MTEM) for estimating activity coefficients of electrolytes and ions in inorganic multicomponent solutions (Zaveri et al., 2005b), the Multicomponent Equilibrium Solver for Aerosols (MESA) to compute intraparticle solid–liquid partitioning (Zaveri et al., 2005a) and a solver for dynamic gas-particle partitioning (Zaveri et al., 2008). To simulate secondary organic aerosol (SOA) we use the Secondary Organic Aerosol Model (SORGAM) scheme (Schell et al., 2001). The CBM-Z gas phase mechanism includes 77 gaseous species. MOSAIC treats key aerosol species including sulfate (SO_4), nitrate (NO_3), ammonium (NH_4), chloride (Cl), carbonate (CO_3), methanesulfonic acid (MSA), sodium (Na), calcium (Ca), other inorganic mass (OIN), black carbon (BC), primary and secondary organic aerosol (POA and SOA). Species such as Cl, Na, Ca, and other mineral components are not included in this study. The simulations were conducted using PartMC version 2.6.1 and MOSAIC version 2019-01-05.

3.2 Synthetic Validation scenario library

The details of the scenario library were described in Liu et al. (2025). In short, the scenario library generated from previous work focuses on urban environments, and in particular on the aging process of carbonaceous aerosol by coagulation and condensation of secondary aerosols, which result in changes in per-particle chemical composition. The simulations were performed in a two-stage process: a spin-up run starting from zero aerosol initial conditions, followed by a second run using randomly selected aerosol populations from the spin-up as initial conditions. Each 48-h simulation featured a diurnal emission pattern starting at 6 AM LST (local solar time), with aerosol and gas phase emissions during the 12 h daytime period, representing a well-mixed, polluted boundary layer. Then we discontinued emissions during the 12 h nighttime period, representing the polluted air remaining in the nocturnal residual layer. We repeated the same process 100 times using different input parameters, yielding

Table 1. Diameter ranges replicate quasi-monodisperse particle selection in HTDMA measurements.

D_{p} (nm)	$D_{\mathrm{p,min}}$ (nm)	$D_{\mathrm{p,max}}$ (nm)
50	47.3	52.6
100	94.2	105.6
150	140.7	159.1
200	186.8	212.9
250	232.7	267.1

4,900 aerosol populations with diverse mixing states and chemical compositions. The input parameter space was constructed using a Latin hypercube sampling approach following the strategy of Zheng et al. (2021).

In this study, we used "N_2O_5-ON" as a synthetic validation library, though N_2O_5 chemistry is not the focus of the current analysis. Note that primary sea salt emissions were not included in the library. Accordingly, the validation results presented here are primarily applicable to continental anthropogenic aerosol regimes. For each population, we first selected particles with dry diameter (D_{p}) within narrow size ranges centered at 50, 100, 150, 200, and 250 nm (Table 1). This procedure mimics HTDMA measurements, in which dry, quasi-monodisperse aerosol particles are selected using a differential mobility analyzer (DMA). We then calculated χ using two approaches. First, we calculated χ^{PMC}, the particle-resolved reference mixing state index, following the mixing-state framework of Riemer and West (2013), using single-particle volume fractions from the PartMC-MOSAIC output, which represents the particle-resolved reference mixing state of each population. For the χ^{PMC} calculation, species were assigned to low- or high-hygroscopic groups. The low-hygroscopic group comprised SOA species represented in SORGAM, including aromatic-derived species (ARO1 and ARO2), alkane-derived species (ALK1), alkene-derived species (OLE1), α-pinene-derived species (API1 and API2), and limonene-derived species (LIM1 and LIM2), as well as OIN, POA, and BC, while the high-hygroscopic group included $\mathrm{SO_4}$, $\mathrm{NO_3}$, Cl, $\mathrm{NH_4}$, MSA, $\mathrm{CO_3}$, Na, and Ca. We then constructed the population-level κ-PDF based on individual particle hygroscopicity parameters κ derived from particle composition using the ZSR mixing rule, and applied the YZ method to obtain χ^{YZ}. The deviation between χ^{PMC} and χ^{YZ} quantifies the systematic bias associated with the YZ method.

4 Evaluation and interpretation of κ-based mixing state indices

In this section, we first quantify the agreement between κ-based and particle-resolved mixing state indices across particle sizes, then examine the physical origin of systematic biases, and finally illustrate the non-uniqueness of bulk hygroscopicity metrics with respect to aerosol mixing state.

4.1 Quantitative comparison of mixing state indices

Figure 1 compares the hygroscopicity-based aerosol mixing state indices estimated from the YZ method (χ^{YZ}) with those computed from single-particle composition data (χ^{PMC}) for five dry diameters (50–250 nm) in the validation scenario library. The value of χ^{PMC} represents the reference mixing state by preserving the chemical composition and hygroscopicity of individual particles. Overall, the YZ method agrees well with the particle-resolved calculations, with a mean absolute error (MAE) of $\sim$2% across all diameters. However, notable overestimations are observed, particularly at 150 nm for more externally mixed populations (χ^{PMC} < 40%), where the maximum bias ($\Delta\chi = \chi^{\mathrm{YZ}} - \chi^{\mathrm{PMC}}$) reaches 29%. It is also worth noting that larger errors are associated with SOA-rich populations.

The retrieval framework assumes a representative hygroscopicity for the inorganic-salt component. To assess the sensitivity of the retrieval to this assumption, we repeated the analysis using κ_{MH} values of 0.60, 0.65, and 0.70 (Figure S1). The sensitivity arises because the inferred MH volume fraction in each κ bin depends directly on the assumed end-member values through Eq. (1). For a given particle hygroscopicity, decreasing κ_{MH} increases the inferred P_{MH} and shifts particles with hygroscopicities near the MH end member closer to pure-MH composition, leading to a systematic underestimation of χ. In contrast, increasing κ_{MH} decreases the inferred P_{MH}, causing particles that would otherwise be assigned closer to the pure-MH end member to be interpreted as mixtures of LH and MH components, resulting in a systematic overestimation of χ. Across particle diameters, the MAE increases from 1.6%–2.4% for the baseline $\kappa_{\mathrm{MH}} = 0.65$ case to 7.2%–11.8% for $\kappa_{\mathrm{MH}} = 0.60$ and 10.5%–17.3% for $\kappa_{\mathrm{MH}} = 0.70$ (Figure S1). Nevertheless, strong correlations are maintained across all tested values, indicating that the retrieval is robust to reasonable uncertainty in the representative hygroscopicity assigned to inorganic salts, although accurate specification of κ_{MH} is important for minimizing systematic bias.

To investigate how the presence of intermediate-hygroscopicity components (e.g., SOA) breaks down the binary assumption, we next examine the κ-PDFs.

4.2 Constructing confidence intervals for χ retrievals

We quantified the uncertainty associated with κ-based mixing state retrievals by computing the retrieval errors ($\Delta\chi = \chi^{\mathrm{YZ}} - \chi^{\mathrm{PMC}}$) from Figure 1 and summarizing its distribution in Figure 2. The retrieval exhibits a systematic positive bias across all particle sizes and the uncertainty (width of the shaded area) increases with diameter. Notably, the error remains within $\pm$10% for χ >70% for all diameters, indicating a reliable retrieval regime for more internally mixed populations. These error distributions are subsequently applied to quantify uncertainties in χ retrieved from long-term HTDMA measurements.

4.3 Systematic bias associated with intermediate-hygroscopicity components

For populations with higher SOA content, the bias in χ depends critically on how the majority of SOA is mixed with other components (Figure 3). A large overestimation of χ occurs when species are segregated into particles (Figure 3a), since a substantial fraction of pure SOA particles that do not fit into either the LH or MH categories introduce the bias. In contrast, when SOA is primarily internally mixed with hygroscopic species (Figure 3b), the bias becomes negligible.

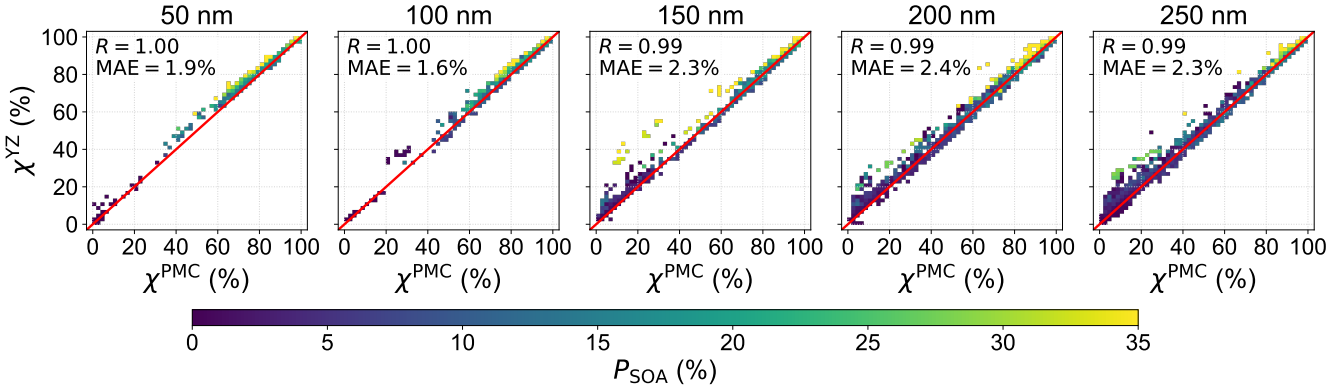

Figure 1. Scatter plots between χ^{YZ} (κ-based mixing state estimates using the YZ method) and χ^{PMC} (mixing state index computed from per-particle composition) for aerosols with dry diameters of 50, 100, 150, 200, 250 nm. Each point represents a particle population from the validation scenario library, with colors indicating the bulk SOA volume fraction (P_{SOA}). The red line shows the 1:1 relationship. Correlation coefficients (R) and mean absolute errors (MAE) are shown in each panel.

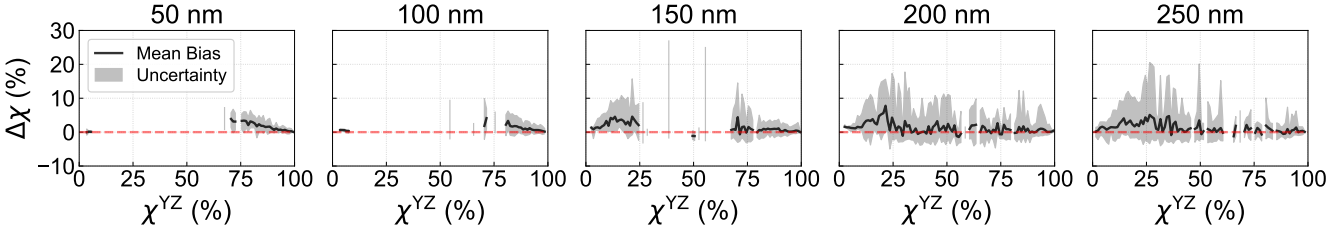

Figure 2. Error distribution of χ retrieval from Figure 1. Solid lines represent the mean bias and shaded areas show the uncertainty range (2.5^{th}–97.5^{th} percentiles of the error). Gaps correspond to χ ranges with insufficient particle samples to estimate statistics.

To illustrate the fundamental limitation of the binary assumption in the YZ method, we constructed two simplified cases. First, consider a fully externally mixed population (Figure 3c) with half the particles pure SOA ($\kappa_{\mathrm{SOA}} = 0.1$) and half pure ammonium sulfate (AS; $\kappa_{\mathrm{AS}} = 0.65$) . Under the binary assumption, the YZ method misinterprets pure SOA particles as artificial mixtures containing 15% MH species and 85% LH species (following Eq. (1): $P_{i,\mathrm{MH}} = (\kappa_{\mathrm{SOA}} - \kappa_{\mathrm{LH}})/(\kappa_{\mathrm{MH}} - \kappa_{\mathrm{LH}}) = (0.1 - 0)/(0.65 - 0) \approx 15\%$). By assigning SOA particles a higher effective number of species than they physically contain, the method estimates a higher average per-particle diversity (D_α), thereby shifting the population toward a more internally mixed state. Alternatively, consider a monodispersed population (Figure 3d) in which each particle is an internal mixture of 50% SOA and 50% AS. In this case, all particles have the same κ of 0.375, resulting in a narrow, unimodal κ-PDF. The YZ method correctly identifies this state ($\chi^{\mathrm{YZ}} = 1$), as the bulk population diversity directly reflects the average per-particle diversity ($D_\gamma = D_\alpha$).

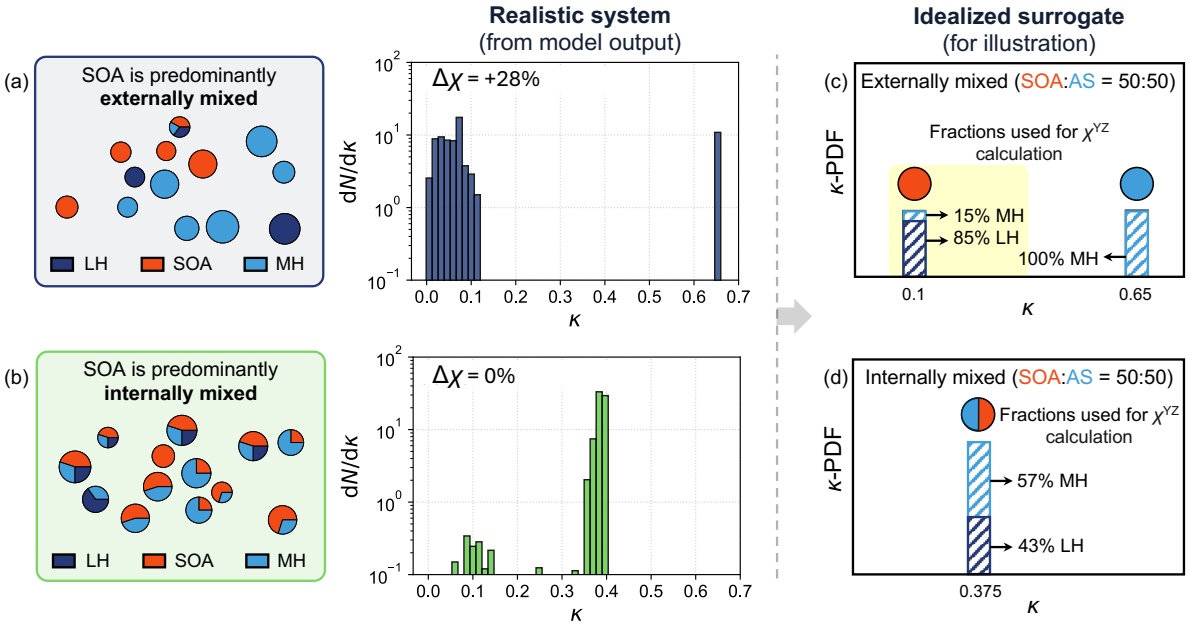

Figure 3. (a and b) Representative PartMC-derived κ-PDFs from the validation scenario library for two aerosol populations with high secondary organic aerosol (SOA) content at a dry diameter of 150 nm, corresponding to predominantly externally mixed (a) and internally mixed (b) particle populations. Note that y-axes are in logarithmic scale. (c and d) Schematic diagrams of idealized surrogate cases with identical bulk compositions of 50% SOA and 50% ammonium sulfate (AS).

These examples demonstrate that systematic overestimation of χ arises specifically when intermediate-hygroscopicity components are externally mixed, causing the κ-based binary mapping to misclassify chemically simple particles as artificial mixtures.

4.4 Non-uniqueness of bulk hygroscopicity with respect to mixing state

Before turning to field applications, we use the particle-resolved simulations to illustrate a more general property of aerosol populations: bulk hygroscopicity alone does not uniquely determine aerosol mixing state. Figure 4 illustrates how aerosol mixing state is encoded in particle-to-particle variability rather than bulk hygroscopicity alone. From the full scenario library, we identified seven populations with a dry diameter of 150 nm that share the same mean hygroscopicity (κ_{mean}=0.31) but differ markedly in their particle-level composition distributions and mixing state indices. This example highlights that even within a narrow size range, particles can exhibit substantial variability in composition, a defining characteristic of aerosol mixing state that the particle-resolved model explicitly resolves.

Because κ_{mean} constrains only the bulk fraction of less- and more-hygroscopic material, these populations are indistinguishable based on κ_{mean} alone. In more externally mixed populations, ($\chi^{\mathrm{pmc}} < 30\%$), the distribution of P_{MH} is dominated by two distinct modes near 0 and 100%, indicating segregation of hygroscopic components among particles. As the popula-

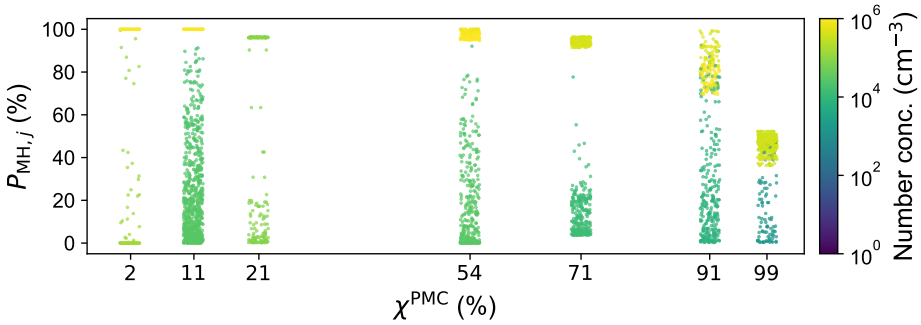

Figure 4. Strip plot of more-hygroscopic (MH) component volume fractions ($P_{\mathrm{MH},j}$) for particles at $D_p = 150$ nm. The seven aerosol populations shown have identical mean hygroscopicity ($\kappa_{\mathrm{mean}} = 0.31$) but different mixing state indices (χ^{PMC}). Each dot represents a particle population from the PartMC simulation, and its color indicates number concentration. Dots are grouped by the χ^{PMC} value of each aerosol population, with a small horizontal jitter applied only for visualization.

tions become increasingly internally mixed ($\chi^{\mathrm{pmc}} \to 1$), these modes broaden and merge, and the distribution of P_{MH} becomes continuous and centered at intermediate values. For nearly fully internally mixed populations, the distinction between subpopulations is effectively lost.

The distinction between aerosol populations with identical κ_{mean} but different mixing states may have important implications for aerosol-cloud interactions. Activation of a particle depends on whether its hygroscopicity is sufficient to lower its critical supersaturation below the ambient supersaturation (Petters and Kreidenweis, 2007). In an externally mixed population (lower χ), a substantial fraction of particles are dominated by less hygroscopic species, such as black carbon or primary organic aerosol, yielding high critical supersaturations that may exceed the maximum supersaturation reached in clouds. These particles are therefore unlikely to activate as cloud condensation nuclei (CCN). In contrast, a more internally mixed population (higher χ) with the same κ_{mean} distributes hygroscopic material more uniformly across all particles, lowering the critical supersaturation for a larger fraction of the population and increasing the number of CCN-active particles. As a result, aerosol populations with similar κ_{mean} but different χ values may exert different indirect radiative effects.

This result is consistent with the conceptual analysis of Yuan and Zhao (2023), and we explicitly demonstrate through particle-resolved simulations that identical mean hygroscopicity can correspond to fundamentally different aerosol mixing states. Information on particle-to-particle variability, as quantified by the mixing state index χ, is therefore required to distinguish aerosol populations with the same κ_{mean}.

5 Mixing state retrievals from long-term HTDMA measurements

Having quantified the performance and limitations of κ-based mixing state retrievals using particle-resolved simulations, we now apply the method to long-term hygroscopicity measurements to examine aerosol mixing state in real atmospheric environments.

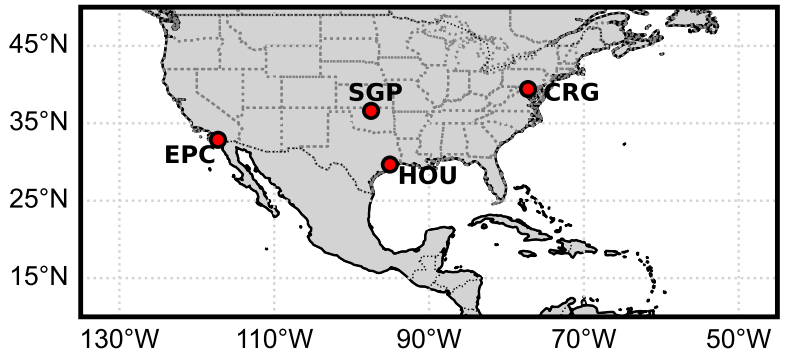

Figure 5. Map of ARM sites with long-term HTDMA measurements: Baltimore, MD (CRG); La Jolla, CA (EPC); Houston, TX (HOU); and Southern Great Plains, OK (SGP).

In this section, we apply the YZ method to multi-year HTDMA datasets (2021–2025) from four U.S. Department of Energy Atmospheric Radiation Measurement (DOE ARM) campaigns (Uin et al., 2012): CoURAGE (CRG), TRACER (HOU), Southern Great Plains (SGP), and EPCAPE (EPC). For each HTDMA dataset, we extracted κ and particle number concentrations at specified dry diameters to construct κ-PDFs, which were then applied in the YZ framework to calculate χ^{YZ}. Figure 5 shows the geographical location of the four ARM sites.

5.1 Typical κ distributions in field measurements

An example of HTDMA-measured κ-PDFs across the four ARM sites is shown in Figure 6, which can be considered as the normalized aerosol number fractions varied with κ between 0 and 0.65. These long-term averaged κ-PDFs are often broad and, in some cases, distinctly multi-modal, indicating substantial particle-to-particle hygroscopicity heterogeneity. Notably, the distributions for 50 nm particles consistently peak at lower κ values and exhibit narrower spreads compared to larger particles across all sites, likely reflecting the greater abundance of freshly emitted, low-hygroscopicity combustion particles.

While the shape and structure of these κ-PDFs provide insight into aerosol mixing state, they do not uniquely determine chemical composition. A given κ value may arise from different combinations of chemical species, and without additional speciation measurements, one cannot reliably attribute a peak in the distribution to a particular aerosol type of chemical component. Therefore, mapping from hygroscopicity distributions to aerosol mixing state is non-trivial and needs careful consideration when making compositional assumptions.

5.2 Long-term χ retrievals from ARM measurements

The time series of χ^{YZ} is shown in Figure 7. For each dry diameter, the shaded uncertainty range is obtained by applying the particle-size-dependent retrieval-error distributions derived from the PartMC-MOSAIC evaluation (Section 4.2; Figure 2) to the corresponding HTDMA-derived χ^{YZ} values. Across all sites and seasons, χ^{YZ} typically falls between 70% and 90%,

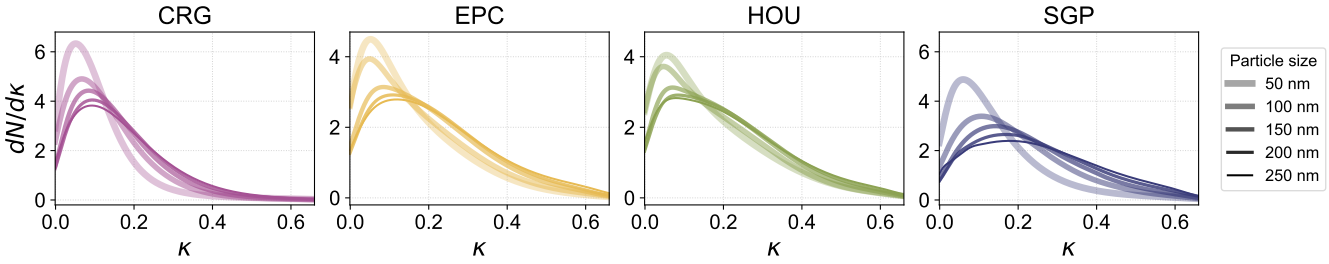

Figure 6. Campaign-averaged κ-PDFs for 50, 100, 150, 200, and 250 nm particles. Each panel represents a different site from the U.S. Department of Energy (DOE) Atmospheric Radiation Measurement (ARM) program: Baltimore, MD (CRG); La Jolla, CA (EPC); Houston, TX (HOU); Southern Great Plains, OK (SGP). Particle sizes are distinguished by opacity, with larger particles shown as more opaque.

a regime where our model evaluation indicates that the κ-based retrieval is generally reliable. Comparable ranges have been reported in Chengdu measurements (60%–90%) using the same method (Yuan and Zhao, 2023). The relatively narrow range of retrieved χ^{YZ} values is notable given the diversity of the four ARM sites and the variability in colocated aerosol and meteorological measurements. It suggests that, for the HTDMA-selected submicron particles considered here, site-specific source and transport effects modulate particle-to-particle hygroscopicity variability within a predominantly intermediate-to-high mixing regime, rather than producing persistently strongly externally mixed populations. This interpretation is consistent with previous studies suggesting substantial atmospheric aging and mixing of submicron aerosol populations (Zhao et al., 2021b; Xue et al., 2024b), although definitions of χ vary among studies and are not necessarily based on LH/MH species.

To place the HTDMA-derived κ distributions and χ^{YZ} retrievals in environmental context, we examined colocated ARM measurements of aerosol size distributions, trace gases, meteorology, wind direction, and bulk submicron aerosol composition derived from the aerosol chemical speciation monitor (ACSM) (Figures S2–S6). These measurements show that the four sites differ substantially in aerosol loading, bulk non-refractory composition, transport patterns, and meteorological conditions. The particle number concentrations in different size range provide context for differences in the CCN-relevant aerosol population (Figure S2), while trace gases and wind direction provide information on source influence and transport (Figure S3–S4). The ACSM measurements further show variability in the relative contributions of organic and inorganic aerosol components (Figure S5). These colocated observations support a qualitative interpretation of site-to-site and seasonal differences in χ^{YZ}, but they are not used as direct inputs to the retrieval because they do not provide particle-resolved composition for the same HTDMA-selected particles.

The site-to-site differences are most apparent at HOU and EPC. The HOU site shows generally lower χ^{YZ} values compared to the other continental sites, consistent with a heterogeneous aerosol population in which fresh urban/industrial emissions coexist with more aged regional aerosol. This coexistence can maintain particle-to-particle differences in hygroscopicity, even if atmospheric processing rapidly ages part of the population (Riemer et al., 2004; Wang et al., 2010). This interpretation is supported by elevated SO_2 concentrations and variability in trace-gas conditions (Figure S3). The ACSM measurements further show enhanced sulfate and reduced organic during summer (Figure S5), consistent with seasonal changes in anthropogenic

emission influences. Farley et al. (2024) reported a broader range of mixing-state index values (5%–95%) for soot-containing particles at HOU. These values are not directly comparable to χ^{YZ} because they are based on a different particle population and a different mixing-state definition. However, both studies point to substantial particle-to-particle heterogeneity at HOU.

At EPC, lower wintertime χ^{YZ} values for larger particles are consistent with seasonal changes in source influence and transport. This interpretation is supported by wintertime enhancements in CO and $\mathrm{SO_2}$ (Figure S3), indicating stronger anthropogenic influence than during summer, together with shifts in prevailing wind direction (Figure S4) and seasonal changes in the relative abundance of different particle-size ranges (Figure S2). Similar to HOU, the enhanced anthropogenic influence likely increases the diversity of aerosol sources and particle compositions, thereby maintaining greater particle-to-particle hygroscopicity variability and reducing χ^{YZ}. The ACSM measurements also show enhanced organic fractions during winter and enhanced sulfate fractions during summer (Figure S5), further indicating seasonal changes in the dominant aerosol sources. At the other sites, the auxiliary measurements also show variability in aerosol loading, meteorology, and bulk composition, but these bulk or population-level measurements do not uniquely determine the particle-level hygroscopicity distributions that control χ^{YZ}.

The ACSM measurements provide useful information on bulk non-refractory submicron composition, including organic and inorganic aerosol fractions (Figure S5), but they do not uniquely identify the composition or mixing state of the HTDMA-selected particles. In particular, ACSM does not directly constrain refractory components such as sea salt and black carbon, and the organic aerosol signal does not distinguish POA from SOA without additional source-apportionment analysis. This limitation is particularly relevant at the coastal or coastal-influenced sites, where marine aerosol may contribute during some periods. We therefore interpret the coastal-site χ^{YZ} retrievals with this additional caveat rather than attributing specific κ modes to sea salt.

5.3 Limitations of the YZ method

The particle-resolved simulations demonstrate that the YZ method provides a useful framework for inferring aerosol mixing state from κ-PDFs, particularly for continental aerosol populations in which the prescribed less- and more-hygroscopic end members provide a reasonable representation of the dominant hygroscopicity range. However, the retrieval is sensitive to how these end members are defined. For typical continental inorganic salts, varying the assumed more-hygroscopic end member within a plausible range ($\kappa_{\mathrm{MH}} = 0.60$–$0.70$) changes the magnitude and sign of the bias but preserves the overall correlation between χ_{YZ} and χ_{PMC} (Figure S1). This indicates that accurate end-member selection is important for minimizing systematic bias, but that modest uncertainty in κ_{MH} does not by itself invalidate the retrieval.

A more fundamental limitation arises when the aerosol population cannot be represented well by a binary less-/more-hygroscopic system. In such cases, κ no longer maps uniquely onto a two-component composition. This ambiguity is most evident when chemically distinct particle types have intermediate hygroscopicities or when additional highly hygroscopic components are present. For example, externally mixed SOA-rich particles can be misinterpreted as artificial LH–MH mixtures, leading to overestimation of χ. Similarly, in marine-influenced environments, submicron sea-salt particles have been observed and may extend the hygroscopicity range beyond that of typical continental inorganic salts (O'Dowd and Smith,

1993; Murphy et al., 1998; Yao et al., 2003; Bian et al., 2019; Murphy et al., 2019). Because sea salt is not included in the present PartMC validation library, the results presented here should not be interpreted as a full validation of the YZ method for marine aerosol populations.

To illustrate the sensitivity of the retrieval to this type of end-member mismatch, we repeated the YZ retrieval using a sea-salt-like more-hygroscopic end member, $\kappa_{\mathrm{MH}} = 1.28$, while retaining the same PartMC aerosol populations as the reference (Figure S7). This test is not intended to represent a realistic marine aerosol simulation. Instead, it shows how the binary retrieval behaves when the assumed upper hygroscopicity end member is shifted beyond the hygroscopicity of common non-sea-salt inorganic species. Under this assumption, sulfate-, nitrate-, and ammonium-rich particles become intermediate relative to the prescribed LH–MH end members and can be interpreted as mixtures, leading to systematic overestimation of χ^{YZ} relative to χ^{PMC}.

These examples highlight the broader non-uniqueness of κ-based mixing-state retrievals. Retrieval uncertainty increases when multiple chemically distinct particle types can produce similar κ values, or when important aerosol components fall outside the assumed end-member range. Applications in coastal, marine-influenced, or SOA-rich environments should therefore be interpreted cautiously, especially when externally mixed intermediate- or highly hygroscopic components are expected. Colocated bulk composition measurements, such as ACSM, provide useful context for the non-refractory submicron aerosol composition, but they do not directly constrain refractory sea-salt mass, particle-resolved composition, or the mixing state of the HTDMA-selected particles.

One possible extension would be to represent aerosol populations using more than two hygroscopicity classes, for example by adding an intermediate-hygroscopicity class for organic aerosol or a highly hygroscopic class for sea salt. Such an extension could reduce some of the biases identified here, because intermediate-hygroscopicity particles would no longer be forced into artificial LH–MH mixtures. However, this would also remove a key advantage of the original YZ framework: in the binary case, the measured κ value constrains the relative LH and MH fractions for each κ bin. Adding additional classes introduces additional unknown component fractions, so the same measured κ value can generally be produced by multiple combinations of those fractions. A multi-class retrieval would therefore require additional observational constraints, such as independent size-resolved composition or source-apportionment information. Developing and evaluating such an extension is beyond the scope of the present work.

Despite these limitations, the YZ method remains useful for aerosol populations in which the dominant hygroscopicity range is reasonably represented by the prescribed LH and MH endmembers and intermediate-hygroscopicity components are not predominantly externally mixed. These conditions are expected to be most common for aged continental and anthropogenic aerosol populations, where condensation, coagulation, and multiphase processing tend to reduce particle-to-particle compositional contrasts. In such cases, κ-PDFs provide a physically meaningful constraint on particle-to-particle hygroscopicity variability, and the YZ framework enables statistically consistent mixing-state inference from long-term HTDMA observations. This is an important advantage because comparable time coverage is difficult to obtain from particle-resolved composition measurements.

6 Conclusions

This study presents a comprehensive evaluation of the hygroscopicity-based aerosol mixing state index (χ) derived from HTDMA measurements using the method proposed by Yuan and Zhao (2023). By enabling aerosol mixing state metrics to be inferred from routinely available hygroscopicity measurements, the approach of Yuan and Zhao (2023) provides an important practical pathway for extending the mixing state analyses to long-term observational datasets. Using a large ensemble of particle-resolved (PartMC–MOSAIC) simulations, we quantify the performance and systematic limitations of inferring χ from κ distributions under realistic atmospheric conditions.

Overall, the YZ method agrees well with PartMC-MOSAIC simulations across a wide range of particle sizes and mixing states (MAE$\sim$2%). Systematic overestimation of χ arises when intermediate-hygroscopicity components, such as secondary organic aerosol, are predominantly externally mixed, violating the binary hygroscopicity assumption that underlies the retrieval. In most atmospheric scenarios, however, including cases where SOA is present but largely internally mixed, the method provides a robust approximation of aerosol mixing state from long-term hygroscopicity measurements, enabling systematic analysis of field datasets where detailed composition information is unavailable. Application to ambient measurements reveals that κ-derived χ values typically range from 70% to 90%, indicating a high degree of internal mixing in observed aerosol populations.

Similarly, the presence of highly hygroscopic species that exceed the upper bound of the assumed binary spectrum (e.g., sea salt with κ>1) requires calibration of the hygroscopicity thresholds, which constrains the hygroscopicity separation among aerosol types and degrades retrieval accuracy. These limitations should be considered when applying the YZ method to aerosol populations dominated by externally mixed intermediate- or highly-hygroscopic species.

The present implementation follows the binary hygroscopicity framework proposed by Yuan and Zhao (2023), in which aerosol populations are represented using prescribed less- and more-hygroscopic end members. In principle, the framework could be extended to include additional hygroscopicity classes or continuous hygroscopicity distributions. Such an extension may improve the representation of aerosol populations containing substantial intermediate-hygroscopicity material and could reduce some of the biases identified in this study. However, introducing additional hygroscopicity classes would also increase the dimensionality of the retrieval and may require additional observational constraints to maintain solution uniqueness. Evaluation of such multi-component retrieval frameworks is beyond the scope of the present work and will be explored in future studies.

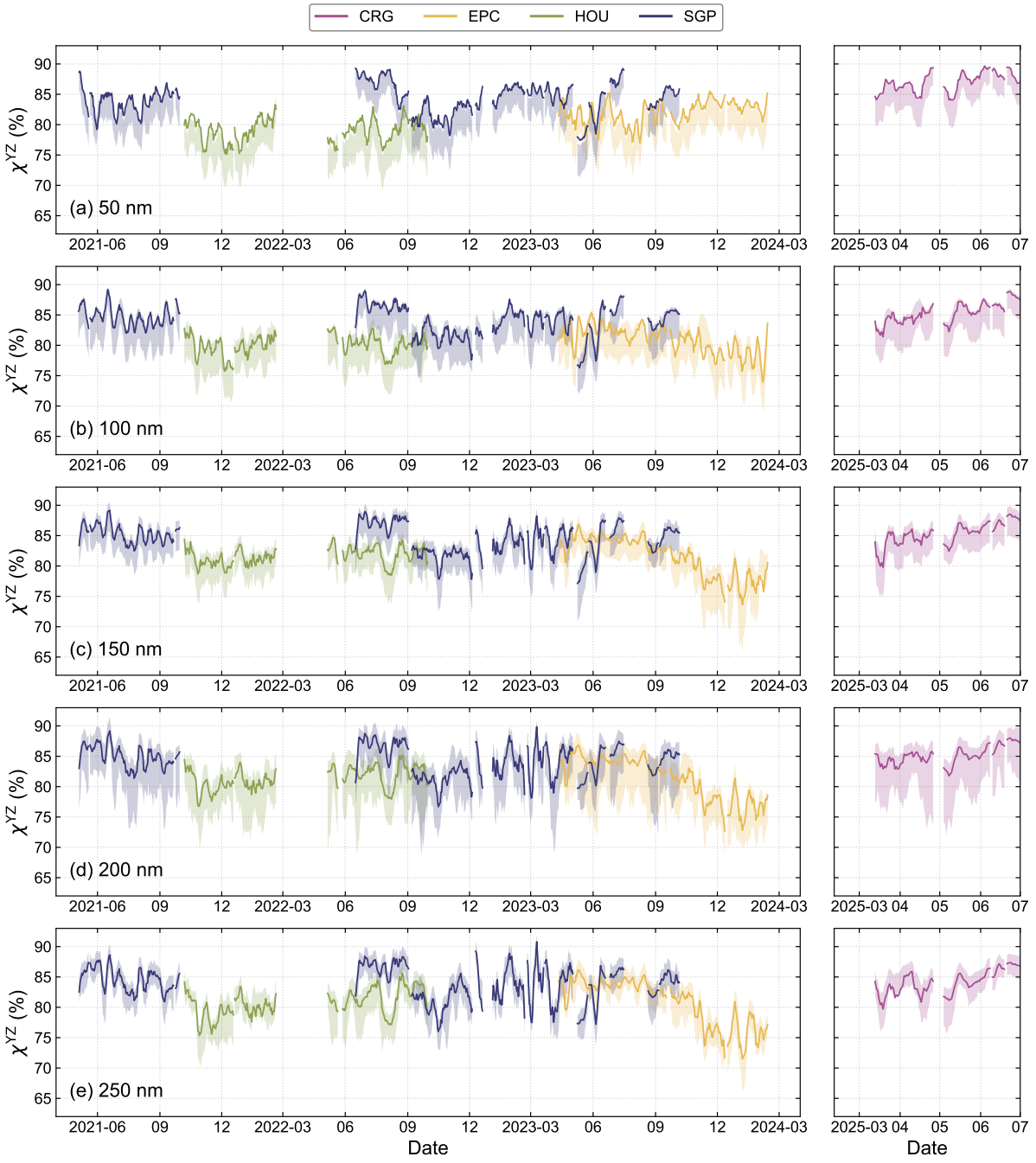

Figure 7. Time series of χ^{YZ} for particles with dry diameters of (a) 50 nm, (b) 100 nm, (c) 150 nm, (d) 200 nm, and (e) 250 nm at four Atmospheric Radiation Measurement (ARM) program sites. Lines represent 7-day moving averages, and shaded areas indicate the 95% range of uncertainty.

Code availability. PartMC v2.6.1 is archived at https://zenodo.org/records/5644422.

Author contributions. YL conducted the data analysis and drafted the manuscript. JW provided guidance on the interpretation of HTDMA measurements and reviewed the manuscript. NR supervised the research and contributed to the study design. All authors contributed to the discussion of the results.

Competing interests. The authors declare that they have no conflict of interest.

Acknowledgements. This work was supported by DOE ASR grant DE-SC0025197.

References

Adachi, K., Tobo, Y., Koike, M., Freitas, G., Zieger, P., and Krejci, R.: Composition and Mixing State of Arctic Aerosol and Cloud Residual Particles from Long-Term Single-Particle Observations at Zeppelin Observatory, Svalbard, Atmospheric Chemistry and Physics, 22, 14 421–14 439, https://doi.org/10.5194/acp-22-14421-2022, 2022.

Adam, M., Putaud, J. P., Martins dos Santos, S., Dell'Acqua, A., and Gruening, C.: Aerosol Hygroscopicity at a Regional Background Site (Ispra) in Northern Italy, Atmospheric Chemistry and Physics, 12, 5703–5717, https://doi.org/10.5194/acp-12-5703-2012, 2012.

Baustian, K. J., Cziczo, D. J., Wise, M. E., Pratt, K. A., Kulkarni, G., Hallar, A. G., and Tolbert, M. A.: Importance of Aerosol Composition, Mixing State, and Morphology for Heterogeneous Ice Nucleation: A Combined Field and Laboratory Approach, Journal of Geophysical Research: Atmospheres, 117, https://doi.org/10.1029/2011JD016784, 2012.

Bian, H., Froyd, K., Murphy, D. M., Dibb, J., Darmenov, A., Chin, M., Colarco, P. R., da Silva, A., Kucsera, T. L., Schill, G., Yu, H., Bui, P., Dollner, M., Weinzierl, B., and Smirnov, A.: Observationally Constrained Analysis of Sea Salt Aerosol in the Marine Atmosphere, Atmospheric Chemistry and Physics, 19, 10 773–10 785, https://doi.org/10.5194/acp-19-10773-2019, 2019.

Bondy, A. L., Bonanno, D., Moffet, R. C., Wang, B., Laskin, A., and Ault, A. P.: The Diverse Chemical Mixing State of Aerosol Particles in the Southeastern United States, Atmospheric Chemistry and Physics, 18, 12 595–12 612, https://doi.org/10.5194/acp-18-12595-2018, 2018.

Brechtel, F. J. and Kreidenweis, S. M.: Predicting Particle Critical Supersaturation from Hygroscopic Growth Measurements in the Humidified TDMA. Part I: Theory and Sensitivity Studies, Journal of the Atmospheric Sciences, 57, 1854–1871, https://doi.org/10.1175/1520-0469(2000)057<1854:PPCSFH>2.0.CO;2, 2000.

Cheng, Z., Morgenstern, M., Henning, S., Zhang, B., Roberts, G. C., Fraund, M., Marcus, M. A., Lata, N. N., Fialho, P., Mazzoleni, L., Wehner, B., Mazzoleni, C., and China, S.: Cloud Condensation Nuclei Activity of Internally Mixed Particle Populations at a Remote Marine Free Troposphere Site in the North Atlantic Ocean, Science of The Total Environment, 904, 166 865, https://doi.org/10.1016/j.scitotenv.2023.166865, 2023.

Collins, D. R., Cocker, D. R., Flagan, R. C., and Seinfeld, J. H.: The Scanning DMA Transfer Function, Aerosol Science and Technology, 38, 833–850, https://doi.org/10.1080/027868290503082, 2004.

Cubison, M. J., Ervens, B., Feingold, G., Docherty, K. S., Ulbrich, I. M., Shields, L., Prather, K., Hering, S., and Jimenez, J. L.: The Influence of Chemical Composition and Mixing State of Los Angeles Urban Aerosol on CCN Number and Cloud Properties, Atmospheric Chemistry and Physics, 8, 5649–5667, https://doi.org/10.5194/acp-8-5649-2008, 2008.

Deshmukh, S., Poulain, L., Wehner, B., Henning, S., Petit, J.-E., Fombelle, P., Favez, O., Herrmann, H., and Pöhlker, M.: External Particle Mixing Influences Hygroscopicity in a Sub-Urban Area, Atmospheric Chemistry and Physics, 25, 741–758, https://doi.org/10.5194/acp-25-741-2025, 2025.

Drame, M. S., Ceamanos, X., Roujean, J. L., Boone, A., Lafore, J. P., Carrer, D., and Geoffroy, O.: On the Importance of Aerosol Composition for Estimating Incoming Solar Radiation: Focus on the Western African Stations of Dakar and Niamey during the Dry Season, Atmosphere, 6, 1608–1632, https://doi.org/10.3390/atmos6111608, 2015.

Ebert, M., Weinbruch, S., Hoffmann, P., and Ortner, H. M.: The Chemical Composition and Complex Refractive Index of Rural and Urban Influenced Aerosols Determined by Individual Particle Analysis, Atmospheric Environment, 38, 6531–6545, https://doi.org/10.1016/j.atmosenv.2004.08.048, 2004.

Farley, R. N., Lee, J. E., Rivellini, L.-H., Lee, A. K. Y., Dal Porto, R., Cappa, C. D., Gorkowski, K., Shawon, A. S. M., Benedict, K. B., Aiken, A. C., Dubey, M. K., and Zhang, Q.: Chemical Properties and Single-Particle Mixing State of Soot Aerosol in Houston during the TRACER Campaign, Atmospheric Chemistry and Physics, 24, 3953–3971, https://doi.org/10.5194/acp-24-3953-2024, 2024.

Fraund, M., Pham, D. Q., Bonanno, D., Harder, T. H., Wang, B., Brito, J., De Sá, S. S., Carbone, S., China, S., Artaxo, P., Martin, S. T., Pöhlker, C., Andreae, M. O., Laskin, A., Gilles, M. K., and Moffet, R. C.: Elemental Mixing State of Aerosol Particles Collected in Central Amazonia during GoAmazon2014/15, Atmosphere, 8, 173, https://doi.org/10.3390/atmos8090173, 2017.

Gasparik, J. T., Ye, Q., Curtis, J. H., Presto, A. A., Donahue, N. M., Sullivan, R. C., West, M., and Riemer, N.: Quantifying Errors in the Aerosol Mixing-State Index Based on Limited Particle Sample Size, Aerosol Science and Technology, 54, 1527–1541, https://doi.org/10.1080/02786826.2020.1804523, 2020.

George, I. J. and Abbatt, J. P. D.: Heterogeneous Oxidation of Atmospheric Aerosol Particles by Gas-Phase Radicals, Nature Chemistry, 2, 713–722, https://doi.org/10.1038/nchem.806, 2010.

H. Bertram, T., E. Cochran, R., H. Grassian, V., and A. Stone, E.: Sea Spray Aerosol Chemical Composition: Elemental and Molecular Mimics for Laboratory Studies of Heterogeneous and Multiphase Reactions, Chemical Society Reviews, 47, 2374–2400, https://doi.org/10.1039/C7CS00008A, 2018.

Hallberg, A., Ogren, J. A., Noone, K. J., Okada, K., Heintzenberg, J., and Svenningsson, I. B.: The Influence of Aerosol Particle Composition on Cloud Droplet Formation, Journal of Atmospheric Chemistry, 19, 153–171, https://doi.org/10.1007/BF00696587, 1994.

Jiang, F., Zheng, Z., Coe, H., Healy, R. M., Poulain, L., Gros, V., Zhang, H., Li, W., Liu, D., West, M., Topping, D., and Riemer, N.: Integrating Simulations and Observations: A Foundation Model for Estimating the Aerosol Mixing State Index, ACS ES&T Air, 2, 877–890, https://doi.org/10.1021/acsestair.4c00329, 2025.

Kleinman, L. I., Springston, S. R., Daum, P. H., Lee, Y.-N., Nunnermacker, L. J., Senum, G. I., Wang, J., Weinstein-Lloyd, J., Alexander, M. L., Hubbe, J., Ortega, J., Canagaratna, M. R., and Jayne, J.: The Time Evolution of Aerosol Composition over the Mexico City Plateau, Atmospheric Chemistry and Physics, 8, 1559–1575, https://doi.org/10.5194/acp-8-1559-2008, 2008.

Laskin, A., Iedema, M. J., and Cowin, J. P.: Quantitative Time-Resolved Monitoring of Nitrate Formation in Sea Salt Particles Using a CCSEM/EDX Single Particle Analysis, Environmental Science & Technology, 36, 4948–4955, https://doi.org/10.1021/es020551k, 2002.

Lata, N. N., Zhang, B., Schum, S., Mazzoleni, L., Brimberry, R., Marcus, M. A., Cantrell, W. H., Fialho, P., Mazzoleni, C., and China, S.: Aerosol Composition, Mixing State, and Phase State of Free Tropospheric Particles and Their Role in Ice Cloud Formation, ACS Earth and Space Chemistry, 5, 3499–3510, https://doi.org/10.1021/acsearthspacechem.1c00315, 2021.

Leck, C. and Svensson, E.: Importance of Aerosol Composition and Mixing State for Cloud Droplet Activation over the Arctic Pack Ice in Summer, Atmospheric Chemistry and Physics, 15, 2545–2568, https://doi.org/10.5194/acp-15-2545-2015, 2015.

Leck, C., Norman, M., Bigg, E. K., and Hillamo, R.: Chemical Composition and Sources of the High Arctic Aerosol Relevant for Cloud Formation, Journal of Geophysical Research: Atmospheres, 107, AAC 1–1–AAC 1–17, https://doi.org/10.1029/2001JD001463, 2002.

Li, W., Shao, L., Wang, Z., Shen, R., Yang, S., and Tang, U.: Size, Composition, and Mixing State of Individual Aerosol Particles in a South China Coastal City, Journal of Environmental Sciences, 22, 561–569, https://doi.org/10.1016/S1001-0742(09)60146-7, 2010.

Li, W., Sun, J., Xu, L., Shi, Z., Riemer, N., Sun, Y., Fu, P., Zhang, J., Lin, Y., Wang, X., Shao, L., Chen, J., Zhang, X., Wang, Z., and Wang, W.: A Conceptual Framework for Mixing Structures in Individual Aerosol Particles, Journal of Geophysical Research: Atmospheres, 121, 13,784–13,798, https://doi.org/10.1002/2016JD025252, 2016.

Liu, Y., Yao, Y., Curtis, J. H., West, M., and Riemer, N.: The Impacts of Aerosol Mixing State on Heterogeneous N_2O_5 Hydrolysis, Aerosol Science and Technology, 59, 402–423, https://doi.org/10.1080/02786826.2024.2443587, 2025.

M. Tomlin, J., Weis, J., P. Veghte, D., China, S., Fraund, M., He, Q., Reicher, N., Li, C., A. Jankowski, K., A. Rivera-Adorno, F., C. Morales, A., Rudich, Y., C. Moffet, R., K. Gilles, M., and Laskin, A.: Chemical Composition and Morphological Analysis of Atmospheric Particles from an Intensive Bonfire Burning Festival, Environmental Science: Atmospheres, 2, 616–633, https://doi.org/10.1039/D2EA00037G, 2022.

Mochida, M., Nishita-Hara, C., Kitamori, Y., Aggarwal, S. G., Kawamura, K., Miura, K., and Takami, A.: Size-Segregated Measurements of Cloud Condensation Nucleus Activity and Hygroscopic Growth for Aerosols at Cape Hedo, Japan, in Spring 2008, Journal of Geophysical Research: Atmospheres, 115, https://doi.org/10.1029/2009JD013216, 2010.

Murphy, D. M., Anderson, J. R., Quinn, P. K., McInnes, L. M., Brechtel, F. J., Kreidenweis, S. M., Middlebrook, A. M., Pósfai, M., Thomson, D. S., and Buseck, P. R.: Influence of Sea-Salt on Aerosol Radiative Properties in the Southern Ocean Marine Boundary Layer, Nature, 392, 62–65, https://doi.org/10.1038/32138, 1998.

Murphy, D. M., Froyd, K. D., Bian, H., Brock, C. A., Dibb, J. E., DiGangi, J. P., Diskin, G., Dollner, M., Kupc, A., Scheuer, E. M., Schill, G. P., Weinzierl, B., Williamson, C. J., and Yu, P.: The Distribution of Sea-Salt Aerosol in the Global Troposphere, Atmospheric Chemistry and Physics, 19, 4093–4104, https://doi.org/10.5194/acp-19-4093-2019, 2019.

O'Brien, R. E., Wang, B., Laskin, A., Riemer, N., West, M., Zhang, Q., Sun, Y., Yu, X.-Y., Alpert, P., Knopf, D. A., Gilles, M. K., and Moffet, R. C.: Chemical Imaging of Ambient Aerosol Particles: Observational Constraints on Mixing State Parameterization, Journal of Geophysical Research: Atmospheres, 120, 9591–9605, https://doi.org/10.1002/2015JD023480, 2015.

O'Dowd, C. D. and Smith, M. H.: Physicochemical Properties of Aerosols over the Northeast Atlantic: Evidence for Wind-Speed-Related Submicron Sea-Salt Aerosol Production, Journal of Geophysical Research: Atmospheres, 98, 1137–1149, https://doi.org/10.1029/92JD02302, 1993.

Patterson, E. M.: Optical Properties of the Crustal Aerosol: Relation to Chemical and Physical Characteristics, Journal of Geophysical Research: Oceans, 86, 3236–3246, https://doi.org/10.1029/JC086iC04p03236, 1981.

Petters, M. D. and Kreidenweis, S. M.: A Single Parameter Representation of Hygroscopic Growth and Cloud Condensation Nucleus Activity, Atmospheric Chemistry and Physics, 7, 1961–1971, https://doi.org/10.5194/acp-7-1961-2007, 2007.

Phillips, B. N., Royalty, T. M., Dawson, K. W., Reed, R., Petters, M. D., and Meskhidze, N.: Hygroscopicity- and Size-Resolved Measurements of Submicron Aerosol on the East Coast of the United States, Journal of Geophysical Research: Atmospheres, 123, 1826–1839, https://doi.org/10.1002/2017JD027702, 2018.

Rader, D. J. and McMurry, P. H.: Application of the Tandem Differential Mobility Analyzer to Studies of Droplet Growth or Evaporation, Journal of Aerosol Science, 17, 771–787, https://doi.org/10.1016/0021-8502(86)90031-5, 1986.

Ravishankara, A. R., Rudich, Y., and Wuebbles, D. J.: Physical Chemistry of Climate Metrics, Chemical Reviews, 115, 3682–3703, https://doi.org/10.1021/acs.chemrev.5b00010, 2015.

Riemer, N. and West, M.: Quantifying Aerosol Mixing State with Entropy and Diversity Measures, Atmospheric Chemistry and Physics, 13, 11 423–11 439, https://doi.org/10.5194/acp-13-11423-2013, 2013.

Riemer, N., Vogel, H., and Vogel, B.: Soot Aging Time Scales in Polluted Regions during Day and Night, Atmospheric Chemistry and Physics, 4, 1885–1893, https://doi.org/10.5194/acp-4-1885-2004, 2004.

Riemer, N., West, M., Zaveri, R. A., and Easter, R. C.: Simulating the Evolution of Soot Mixing State with a Particle-resolved Aerosol Model, Journal of Geophysical Research, 114, D09 202, https://doi.org/10.1029/2008JD011073, 2009.

Rivera-Adorno, F. A., Tomlin, J. M., Lata, N. N., Azzarello, L., Robinson, M. A., Washenfelder, R. A., Franchin, A., Middlebrook, A. M., China, S., Brown, S. S., Young, C. J., Fraund, M., Moffet, R. C., and Laskin, A.: Chemical Imaging of Atmospheric Biomass Burning Particles from North American Wildfires, ACS ES&T Air, 2, 508–521, https://doi.org/10.1021/acsestair.4c00242, 2025.

Schell, B., Ackermann, I. J., Hass, H., Binkowski, F. S., and Ebel, A.: Modeling the Formation of Secondary Organic Aerosol within a Comprehensive Air Quality Model System, Journal of Geophysical Research: Atmospheres, 106, 28 275–28 293, https://doi.org/10.1029/2001JD000384, 2001.

Sharpe, S., Li, Y., Benjemia, S., Rivera-Adorno, F., Olayemi, T., Ese, J., Shen, X., Fraund, M., Moffet, R., Nahar Lata, N., Cheng, Z., China, S., R. Homeyer, C., Dykema, J., A. Marcus, M., Wang, J., Cziczo, D., Keutsch, F., and Laskin, A.: Chemical Imaging of Individual Stratospheric Particles Sampled over North America, Environmental Science: Atmospheres, https://doi.org/10.1039/D5EA00127G, 2025.

Shou, C., Riemer, N., Onasch, T. B., Sedlacek, A. J., Lambe, A. T., Lewis, E. R., Davidovits, P., and West, M.: Mixing State Evolution of Agglomerating Particles in an Aerosol Chamber: Comparison of Measurements and Particle-Resolved Simulations, Aerosol Science and Technology, 53, 1229–1243, https://doi.org/10.1080/02786826.2019.1661959, 2019.

Singh, N., Banerjee, T., Deboudt, K., Chakraborty, A., Khan, M. F., and Latif, M. T.: Sources, Composition, and Mixing State of Submicron Particulates over the Central Indo-Gangetic Plain, ACS Earth and Space Chemistry, 5, 2052–2065, https://doi.org/10.1021/acsearthspacechem.1c00130, 2021.

Sun, Y., Wang, Z., Fu, P., Jiang, Q., Yang, T., Li, J., and Ge, X.: The Impact of Relative Humidity on Aerosol Composition and Evolution Processes during Wintertime in Beijing, China, Atmospheric Environment, 77, 927–934, https://doi.org/10.1016/j.atmosenv.2013.06.019, 2013.

Tao, J., Kuang, Y., Luo, B., Liu, L., Xu, H., Ma, N., Liu, P., Xue, B., Zhai, M., Xu, W., Xu, W., and Sun, Y.: Kinetic Limitations Affect Cloud Condensation Nuclei Activity Measurements Under Low Supersaturation, Geophysical Research Letters, 50, e2022GL101 603, https://doi.org/10.1029/2022GL101603, 2023.

Uin, J., Cromwell, E., Hayes, C., and Salwen, C.: Atmospheric Radiation Measurement (ARM) User Facility. Humidified Tandem Differential Mobility Analyzer (AOSHTDMA), updated daily. 2025-03-13 to 2025-11-30, ARM Mobile Facility (CRG), Baltimore, MD: Supplemental Facility 2 in rural setting (S2); 2023-02-15 to 2024-02-13, ARM Mobile Facility (EPC), La Jolla, CA: AMF1 (main site for EPCAPE on Scripps Pier) (M1); 2021-10-01 to 2022-09-30, ARM Mobile Facility (HOU), Houston, TX: AMF1 (main site for TRACER) (M1); 2021-04-27 to 2023-10-24, Southern Great Plains (SGP), Lamont, OK (Extended and Co-located with C1) (E13). Compiled by Uin, J., Cromwell, E., Hayes, C., and Salwen, C. Data set accessed 2025-08-06 at https://doi.org/10.5439/1776643, 2012.

Wang, J., Cubison, M. J., Aiken, A. C., Jimenez, J. L., and Collins, D. R.: The Importance of Aerosol Mixing State and Size-Resolved Composition on CCN Concentration and the Variation of the Importance with Atmospheric Aging of Aerosols, Atmospheric Chemistry and Physics, 10, 7267–7283, https://doi.org/10.5194/acp-10-7267-2010, 2010.

Wang, Y. and Chen, Y.: Significant Climate Impact of Highly Hygroscopic Atmospheric Aerosols in Delhi, India, Geophysical Research Letters, 46, 5535–5545, https://doi.org/10.1029/2019GL082339, 2019.

Wu, J., Liu, J., Gunsch, M. J., Mirrielees, J. A., Moffett, C. E., Zhang, Q., Sheesley, R. J., and Pratt, K. A.: Quantifying the Diversity of an Atmospheric Aerosol Population in an Arctic Oil Field on a Single-Particle Level, Journal of Geophysical Research: Atmospheres, 129, e2024JD041 001, https://doi.org/10.1029/2024JD041001, 2024.

Xue, J., Zhang, T., Park, K., Yan, J., Yoon, Y. J., Park, J., and Wang, B.: Diverse Sources and Aging Change the Mixing State and Ice Nucleation Properties of Aerosol Particles over the Western Pacific and Southern Ocean, Atmospheric Chemistry and Physics, 24, 7731–7754, https://doi.org/10.5194/acp-24-7731-2024, 2024a.

Xue, J., Zhang, T., Park, K., Yan, J., Yoon, Y. J., Park, J., and Wang, B.: Diverse Sources and Aging Change the Mixing State and Ice Nucleation Properties of Aerosol Particles over the Western Pacific and Southern Ocean, Atmospheric Chemistry and Physics, 24, 7731–7754, https://doi.org/10.5194/acp-24-7731-2024, 2024b.

Yao, X., Fang, M., and Chan, C. K.: The Size Dependence of Chloride Depletion in Fine and Coarse Sea-Salt Particles, Atmospheric Environment, 37, 743–751, https://doi.org/10.1016/S1352-2310(02)00955-X, 2003.

Yao, Y., Curtis, J. H., Ching, J., Zheng, Z., and Riemer, N.: Quantifying the Effects of Mixing State on Aerosol Optical Properties, Atmospheric Chemistry and Physics, 22, 9265–9282, https://doi.org/10.5194/acp-22-9265-2022, 2022.

Yeung, M. C., Lee, B. P., Li, Y. J., and Chan, C. K.: Simultaneous HTDMA and HR-ToF-AMS Measurements at the HKUST Supersite in Hong Kong in 2011, Journal of Geophysical Research: Atmospheres, 119, 9864–9883, https://doi.org/10.1002/2013JD021146, 2014.

Yoo, H., Wu, L., Geng, H., and Ro, C.-U.: Physicochemical and Temporal Characteristics of Individual Atmospheric Aerosol Particles in Urban Seoul during KORUS-AQ Campaign: Insights from Single-Particle Analysis, Atmospheric Chemistry and Physics, 24, 853–867, https://doi.org/10.5194/acp-24-853-2024, 2024.

Yu, C., Liu, D., Broda, K., Joshi, R., Olfert, J., Sun, Y., Fu, P., Coe, H., and Allan, J. D.: Characterising Mass-Resolved Mixing State of Black Carbon in Beijing Using a Morphology-Independent Measurement Method, Atmospheric Chemistry and Physics, 20, 3645–3661, https://doi.org/10.5194/acp-20-3645-2020, 2020.

Yuan, L. and Zhao, C.: Quantifying Particle-to-Particle Heterogeneity in Aerosol Hygroscopicity, Atmospheric Chemistry and Physics, 23, 3195–3205, https://doi.org/10.5194/acp-23-3195-2023, 2023.

Zaveri, R. A. and Peters, L. K.: A New Lumped Structure Photochemical Mechanism for Large-Scale Applications, Journal of Geophysical Research: Atmospheres, 104, 30 387–30 415, https://doi.org/10.1029/1999JD900876, 1999.

Zaveri, R. A., Easter, R. C., and Peters, L. K.: A Computationally Efficient Multicomponent Equilibrium Solver for Aerosols (MESA), Journal of Geophysical Research: Atmospheres, 110, https://doi.org/10.1029/2004JD005618, 2005a.

Zaveri, R. A., Easter, R. C., and Wexler, A. S.: A New Method for Multicomponent Activity Coefficients of Electrolytes in Aqueous Atmospheric Aerosols, Journal of Geophysical Research: Atmospheres, 110, https://doi.org/10.1029/2004JD004681, 2005b.

Zaveri, R. A., Easter, R. C., Fast, J. D., and Peters, L. K.: Model for Simulating Aerosol Interactions and Chemistry (MOSAIC), Journal of Geophysical Research: Atmospheres, 113, https://doi.org/10.1029/2007JD008782, 2008.

Zeng, L., Tan, T., Zhao, G., Du, Z., Hu, S., Shang, D., and Hu, M.: Overestimation of Black Carbon Light Absorption Due to Mixing State Heterogeneity, npj Climate and Atmospheric Science, 7, 2, https://doi.org/10.1038/s41612-023-00535-8, 2024.

Zhang, F., Wang, Y., Peng, J., Ren, J., Collins, D., Zhang, R., Sun, Y., Yang, X., and Li, Z.: Uncertainty in Predicting CCN Activity of Aged and Primary Aerosols, Journal of Geophysical Research: Atmospheres, 122, 11,723–11,736, https://doi.org/10.1002/2017JD027058, 2017.

Zhang, Z., Wang, J., Wang, J., Riemer, N., Liu, C., Jin, Y., Tian, Z., Cai, J., Cheng, Y., Chen, G., Wang, B., Wang, S., and Ding, A.: Steady-State Mixing State of Black Carbon Aerosols from a Particle-Resolved Model, Atmospheric Chemistry and Physics, 25, 1869–1881, https://doi.org/10.5194/acp-25-1869-2025, 2025.

Zhao, G., Tan, T., Zhu, Y., Hu, M., and Zhao, C.: Method to Quantify Black Carbon Aerosol Light Absorption Enhancement with a Mixing State Index, Atmospheric Chemistry and Physics, 21, 18 055–18 063, https://doi.org/10.5194/acp-21-18055-2021, 2021a.

Zhao, G., Tan, T., Zhu, Y., Hu, M., and Zhao, C.: Method to Quantify Black Carbon Aerosol Light Absorption Enhancement with a Mixing State Index, Atmospheric Chemistry and Physics, 21, 18 055–18 063, https://doi.org/10.5194/acp-21-18055-2021, 2021b.

Zheng, Z., West, M., Zhao, L., Ma, P.-L., Liu, X., and Riemer, N.: Quantifying the Structural Uncertainty of the Aerosol Mixing State Representation in a Modal Model, Atmospheric Chemistry and Physics, 21, 17 727–17 741, https://doi.org/10.5194/acp-21-17727-2021, 2021.

Zhu, S., Sartelet, K. N., Healy, R. M., and Wenger, J. C.: Simulation of Particle Diversity and Mixing State over Greater Paris: A Model–Measurement Inter-Comparison, Faraday Discussions, 189, 547–566, https://doi.org/10.1039/C5FD00175G, 2016.